JOC The Journal of Organic Chemistry

Article

pubs.acs.org/joc

[2]Pseudorotaxane Formation with FRET Based Luminescence Response: Demonstration of Boolean Operations through Self-Sorting on Solid Surface

Monalisa Gangopadhyay,[†] Arunava Maity,[†] Ananta Dey,[†] and Amitava Das*[,†,‡]

[†]Organic Chemistry Division, CSIR-National Chemical Laboratory, Dr. Homi Bhabha Road, Pune, Maharashtra 411008, India

[‡]CSIR-Central Salt & Marine Chemicals Research Institute, Gijubhai Badheka Marg, Bhavnagar,Gujarat 364002, India

Supporting Information

ABSTRACT: Binary pseudorotaxane formation between an aza crown derivative as host (**H**) and two different imidazolium derivatives as guests ($\mathbf{G_1}$ and $\mathbf{G_2}$) have been studied in detail by NMR (^{1}H NMR, 2D NOESY), optical (steady state electronic and emission spectroscopy), and mass spectroscopy. Binding stoichiometry (1:1), association constant for the respective [2]pseudorotaxane formation ($K_a^{\mathbf{H.G_1}} = (2.61 \pm 0.015) \times 10^3$ M^{-1} and $K_a^{\mathbf{H.G_2}} = (1.27 \pm 0.16) \times 10^3$ M^{-1}), and associated thermodynamic parameters are also evaluated based on isothermal titration calorimetric (ITC) studies. FRET based *luminescence ON* responses are observed on formation of the binary pseudorotaxane ($\mathbf{H.G_1}$ and $\mathbf{H.G_2}$) in a nonpolar medium like dichloromethane. The thermodynamic feasibility of such an energy transfer process is also examined. The higher affinity of **H** and 18-crown-6 toward K^+, as compared to those toward $\mathbf{G_1}$ or $\mathbf{G_2}$, and the reversibility in the host–guest binding process are utilized in demonstrating the self-sorting phenomena with associated changes in luminescence responses that could be correlated for Boolean operators like YES, INHIBIT, OR, and AND gates.

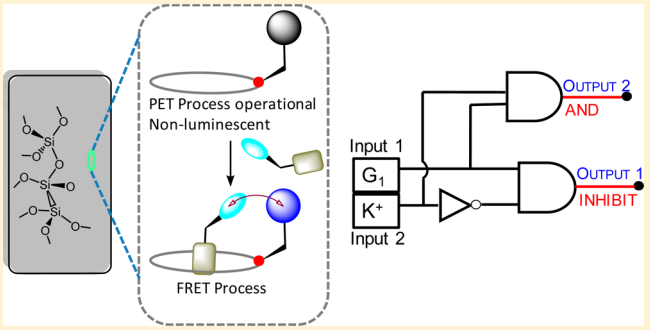

INTRODUCTION

Supramolecular assembly formation primarily relies on molecular recognition phemonena.[1]Thermodynamic stabilities of such assemblies are aided by certain nonbonding interactions like [C–H···O]/[C–H···$N_{[NHR_1R_2]^+}$] and [C–H···π]/[π–π].[1b] Utilization of such a recognition process for developing nanoscopic devices has been the recent focus among researchers who are active in developing functional assemblies, pseudorotaxanes, rotaxanes, and interlocked molecules.[2] Pseudorotaxanes with guest and/or host molecules, appropriately functionalized with photoactive unit(s), are found to have significance for molecular switches, logic gates, shafts, and machines.[3,4] Assembly and deassembly processes associated with such reversible pseudorotaxane formation from individual host and guest components could be achieved in the presence of an external stimulus like acidity/polarity of media or in the presence of certain ionic inputs. Formation of such a threaded or inclusion complex restricts movement(s) of individual component(s). Achieving control in such intercomponent movement(s) in a programmed fashion can actually help in mimicking the function of machines at a molecular level. Presence of an appropriate luminophore, suitably functionalized with host and/or guest fragment(s), offers the possibility of monitoring such processes based on change(s) in luminescence response(s). Förster resonance energy transfer (FRET) is a prevalent photophysical process that involves the transfer of excitation energy of an electronically excited donor molecule to an acceptor molecule at the ground state via a nonradiative process.[5] Spectral overlap (overlap between donor emission and acceptor absorption), distance of separation and relative spatial orientations of the donor and acceptor moieties are crucial in achieving such FRET based responses. Thus, host and guest molecules with appropriately functionalized luminophores that belong to a FRET pair offer the option to monitor such pseudorotaxane formation by probing the FRET based luminescence responses. Importantly, the time scale for luminescence process(es) for most organic fluorophores generally lies within the nano- or picosecond time domain, which is relatively much faster than the time scales for the conformational transitions. However, use of the fluorescence based responses for monitoring the formation of the threaded complex or [2]pseudorotaxane as well as the associated conformational changes of the individual host or guest molecules on a supramolecular assembly formation is rather limited compared to other commonly used techniques like ^{1}H NMR spectroscopy and single crystal X-ray crystallography.[6a]

Crown ether containing aromatic units offers possibilities of weak interactions like hydrogen-bonding, π-stacking, cation–π, and ion–dipole interactions. Use of imidazolium derivatives as

Received: July 7, 2016
Published: September 7, 2016

DOI: 10.1021/acs.joc.6b01631
J. Org. Chem. 2016, 81, 8977–8987

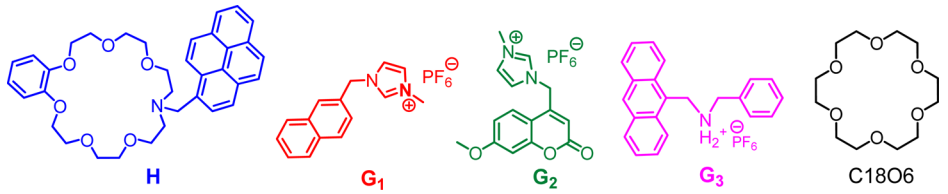

Figure 1. Schematic representation of the molecular components that are used for the formation of [2]pseudorotaxane.

a suitable guest for inclusion complex formation was demonstrated with macrocyclic hosts such as crown ether, cucurbituril, and pillararene derivatives etc.[6] Lehn and his co-workers were first to show that a chiral 1,2,10,11,19,20-hexacarboxylate-27-crown-9 derivative formed a relatively stable complex (K_a (binding constant) of 350 M^{-1}), with an imidazolium ion in aqueous solutions.[7] Further reports from various research groups had established that benzimidazolium derivatives could penetrate the cavity of dibenzo-24-crown-8 macrocycles to produce a new family of [2]pseudorotaxanes.[8] Gibson et al. reported that alkylimidazolium ethane salts with alkyl substituent formed inclusion complexes with dibenzo-24-crown-8 ether (DBC24O8) as a host.[9] These reports reveal that supramolecular structures are stabilized by a series of charge assisted hydrogen bonds ($N^+_{imidazolium}$–H···O), ion–dipole, and π-stacking interactions, where all such host–guest threaded structures are essentially confirmed by single crystal structural analysis. Association constants for formation of various host–guest complexes between DBC24O8 and various imidazolium ions are low (~20–30 M^{-1} in nonpolar or polar aprotic solvents). However, much higher association constants (K_a = 4200–7500 M^{-1}) in water are reported for [2]pseudorotaxane formation between *N*,*N*′-disubstituted (benzyl or phenyl) methylene diimidazolium salts as guest and various macrocycles like β-cyclodextrin, cucurbit[7]uril, tetrapropoxycalix[4]arene, and pillar[5]arenes as hosts.[10] More recently, studies with *N*-alkylated imidazolium derivatives with varying alkyl chain length as guest and DBC24O8 derivative as host reveal that the extent of unfolding of the DBC24O8 crown ether fragment on host–guest adduct formation varies with length of the alkyl chain. Interestingly, appropriate choice of the two fluorophore moieties in DBC24O8 crown ether derivatives helped in probing the unfolding phenomenon of the DBC24O8 crown ether derivative by monitoring the modified luminescence responses owing to the distance dependent one-step FRET process.[11a] Further study with a thread molecule having an additional fluorophore reveals that it is also possible to modulate the luminescence responses through a two-step FRET process in inclusion complex formation.[11b]

Separate studies with secondary ammonium ion derivative as guest and NO_6 based aza-crown derivatives as host, with host/guest molecules functionalized with appropriate FRET pair, reveal that the extent of inclusion complex formation could be linked to the FRET based luminescence responses.[12a] An analysis of all these results leaves us with an impression that perhaps the difference in the affinity constants for the inclusion complex formation as well as the functionalization of the guest fragments with suitable FRET pairs could help us in achieving self-sorting phenomena with different self-assembled inclusion complexes that show modified fluorescence responses for describing a Boolean logic operation.[12b] To the best of our knowledge demonstration of such a logic operation for pseudorotaxane formation is not common and only restricted to studies in solution phase.[13,12b] A variety of inclusion complexes have been explored by utilizing the synthetic self-sorting systems with binding motifs designed on the basis of hydrogen-bonding, metal–ligand, and π–π-stacking interactions.[14−16]

In this article, we report the formation of two different [2]pseudorotaxanes (**H**.$\mathbf{G_1}$ and **H**.$\mathbf{G_2}$) in a nonpolar medium like dichloromethane (Figure 1). A NO_6-aza crown ether derivative (**H**) functionalized with a pyrene moiety is used as the host molecule, while imidazolium ion derivatives having a naphthalene ($\mathbf{G_1}$) or coumarin ($\mathbf{G_2}$) moiety are used as guest molecules. Pyrene moiety is known to form FRET pairs with naphthalene as well as coumarin. This enabled us to achieve two different FRET based luminescence responses for two different inclusion complexes (**H**.$\mathbf{G_1}$ and **H**.$\mathbf{G_2}$). We have further utilized the higher affinity of the aza crown ether moiety (**H**) toward K^+ for preferential formation of the coordination complex **H**.K^+ for demonstration of the Boolean logic operation on a solid surface. To the best of our knowledge such an example is scarce in contemporary literature.

RESULTS AND DISCUSSION

Previously reported methodologies were adopted for the synthesis of **H**, $\mathbf{G_1}$, and $\mathbf{G_3}$.[12a,18b] Synthesis of imidazolium derivative ($\mathbf{G_2}$) is described in the Experimental Section. The desired purity of **H**, $\mathbf{G_1}$, $\mathbf{G_2}$, and $\mathbf{G_3}$ was ensured based on various analytical and spectroscopic data, which are provided either in the Experimental Section or in the Supporting Information section (Figures S1–S4). The inclusion complex formation between **H** and $\mathbf{G_1}$ or $\mathbf{G_2}$ was examined in detail by ^{1}H and ^{13}C NMR spectroscopy. Thermodynamic parameters for the inclusion complex formation were evaluated using data obtained from ITC studies. The luminescence properties of the individual host, guest, and inclusion complexes were investigated by steady state and time-resolved emission studies. Energies of the highest occupied and lowest unoccupied molecular orbitals for individual host and guest molecules were evaluated from their respective ground state redox potential and spectroscopic data.

Photophysical Studies. The absorption spectrum of $\mathbf{G_1}$ in dichloromethane showed an intense absorption band (ε = 2.4 × 10^4 L mol^{-1} cm^{-1}) with a maximum at 280 nm (Figure S5a). The absorption spectrum of **H** was also recorded in dichloromethane, and this revealed three maxima at 314 (ε = 1.14 × 10^4 L mol^{-1} cm^{-1}), 328 (ε = 2.65 × 10^4 L mol^{-1} cm^{-1}), and 344 nm (ε = 3.89 × 10^4 L mol^{-1} cm^{-1}) (Figure S6). The absorption spectrum recorded for a 1:1 mixture of **H** and $\mathbf{G_1}$ in dichloromethane medium was basically a summation of the individual spectra of **H** and $\mathbf{G_1}$ (Figure S7). This suggests that there was no significant interaction between host and guest molecules in the ground electronic state on an assembly formation. The host molecule **H** showed very weak emission bands at 378, 397, and 416 nm, which are characteristic of the pyrene moiety on excitation at any one of these three (314,

DOI: 10.1021/acs.joc.6b01631
J. Org. Chem. 2016, 81, 8977–8987

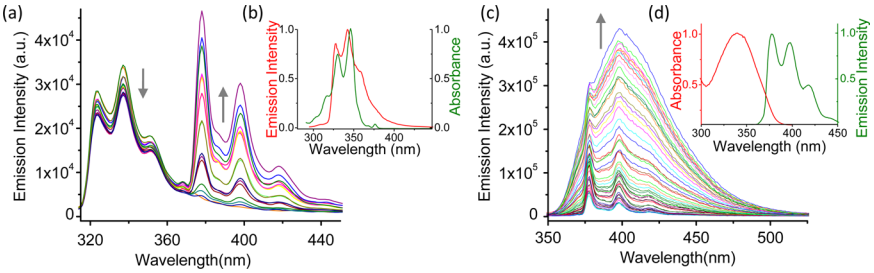

Figure 2. (a) Fluorescence spectra of $\mathbf{G_1}$ (2.0×10^{-7} M), in dichloromethane upon addition of increasing concentration of **H** = (0−8.3×10^{-5} M), λ_{ext} = 277 nm, slit-1/1. (b) Overlap spectra for the emission spectrum of $\mathbf{G_1}$ (red) and absorption spectrum of **H** (green). (c) Changes in luminescence spectral pattern of **H** (1.68×10^{-6} M) on addition of increasing amounts of $\mathbf{G_2}$ (0−8.3×10^{-5} M). λ_{ext} = 314 nm, slit-1/1. (d) Overlap spectra for the emission spectrum of **H** (green) and absorption spectrum of $\mathbf{G_2}$ (red).

328, and 344 nm). This poor emission quantum yield data (Φ = 0.009; evaluated using pyrene as the standard) of **H** is ascribed to the photoinduced electron transfer (PET) process involving the lone pairs of electrons of the tertiary N_{amine}-atom of the NO_6-aza crown ether as the donor moiety to the π system of the photoexcited pyrene unit.[12a,17] The fluorescence spectrum for $\mathbf{G_1}$ in dichloromethane medium shows a band at 340 nm (Φ = 0.229; λ_{ext} = 277 nm; naphthalene was used as reference) (Figure 2b). Interestingly, the emission spectrum of $\mathbf{G_1}$ has a substantial spectral overlap with the electronic spectrum of **H** (Figure 2b), which is one of the essential prerequisites for a probable FRET process that could be operational between two interacting fluorophores. Other factors for an efficient FRET process are the favorable distance between the donor and acceptor (10−100 Å) and their suitable spatial orientation for achieving the appropriate orientation of the transition dipole of the donor and acceptor fluorophores.[5b]

In order to check the possibility of any inclusion complex formation between **H** and $\mathbf{G_1}$ and any plausible FRET based emission response involving the donor (naphthalene in $\mathbf{G_1}$) and acceptor (pyrene in **H**) fluorophores, an equimolar mixture of two molecular components ($\mathbf{G_1}$ and **H**) was allowed to mix in CH_2Cl_2 medium. This solution on excitation with 277 nm (naphthalene absorbed predominantly at this wavelength) showed distinct pyrene based emission bands in the region 378 to 420 nm, which could only be explained on the basis of a FRET based energy transfer. A control experiment performed with an equimolar mixture of **H** and unsubstituted naphthalene imidazolium guest did not show any such FRET based emission response under identical experimental conditions (Figure S8). This tends to suggest a host−guest adduct formation with appropriate spatial orientation that favors the FRET process. 1,3-Disubstituted imidazolium salt is known to form an inclusion complex with DBC24O8 or its derivatives through intermolecular H-bond formation.[10,18]Observed FRET based emission response also supported the formation of such an inclusion complex. H-bonding interactions were important for inclusion complex formation, and such interactions involved the lone pairs of electron of the tertiary nitrogen of the aza-crown ether moiety with effective interruption of the PET process that was initially responsible for the low emission quantum yield of the pyrene moiety in **H**. Interestingly, a substantially low emission quantum yield was observed for naphthalene moiety (Φ = 0.04 for λ_{ext} = 277 nm) when $\mathbf{G_1}$:**H** molar ratio was ∼1:20. This revealed that the emission of the donor naphthalene moiety of $\mathbf{G_1}$ in inclusion complex ($\mathbf{H.G_1}$) was substantially low as compared to that for $\mathbf{G_1}$ alone. Systematic emission titration in CH_2Cl_2 medium (λ_{ext} = 277 nm) revealed a gradual decrease in naphthalene based emission with concomitant increase in pyrene based emission for increasing [**H**]. It is worth mentioning here that, at 277 nm, naphthalene moiety was predominantly excited.

Emission spectrum for **H** alone in CH_2Cl_2 was also recorded using λ_{ext} = 277 nm, which showed a much weaker emission as compared to what was observed for $\mathbf{H.G_1}$ for any comparable concentration of **H** (Figure S9). These observations further corroborated our presumption about the FRET process for the possible inclusion complex $\mathbf{H.G_1}$. Sensitized emission of the acceptor fluorophore (pyrene) with increased quantum yield (Φ = 0.059; λ_{ext} = 277 nm) suggested an efficient FRET process involving naphthalene (in $\mathbf{G_1}$) as donor and pyrene (in **H**) as acceptor on formation of a host−guest adduct ($\mathbf{H.G_1}$) formation (Figure 2a). Absence of any FRET based emission response for control experiments confirmed that the H-bonding interactions in $\mathbf{H.G_1}$ not only stabilized the adduct formation but also favored the appropriate spatial orientation of the donor and acceptor fluorophores for an efficient FRET process.

Optical spectral studies with $\mathbf{G_2}$ revealed absorption and emission bands with maxima at 340 and 400 nm (λ_{ext} of 340 nm) (Figure S5b), respectively, and the absorption band showed a definite spectral overlap with the emission spectrum of **H**: a prerequisite for FRET based emission responses on formation of a possible host−guest adduct $\mathbf{H.G_2}$ (Figure 2d). Analogous studies, as performed with $\mathbf{G_1}$, were also performed with **H** as host and $\mathbf{G_2}$ as guest molecules in identical experimental conditions. Emission titrations were performed in CH_2Cl_2 medium maintaining [**H**] (1.68×10^{-6} M) unchanged with varying [$\mathbf{G_2}$] (0−8.3×10^{-5} M). This showed a steady growth in emission intensity with a maximum at 400 nm (λ_{ext} = 314 nm) on gradual increase in [$\mathbf{G_2}$]. It is worth mentioning that pyrene moiety is predominantly excited on excitation at 314 nm. Emission spectra recorded for pure $\mathbf{G_2}$ in CH_2Cl_2 solution (using λ_{ext} = 314 nm) for any comparable concentration of $\mathbf{G_2}$ were much weaker. Further, the possible decrease in the emission band for the donor pyrene moiety in $\mathbf{H.G_2}$ was masked by the more prominent increase in the emission band of the coumarin moiety (Figure 2c). Figure 2d clearly reveals that the coumarin moiety in $\mathbf{G_2}$ has no significant absorption at 314 nm. All these data and the observed enhancement in coumarin-based emission (Φ = 0.21) (compared to that for pure $\mathbf{G_2}$, Φ = 0.076) on preferential excitation of the pyrene fragment at 314 nm in the hydrogen-bonded adduct $\mathbf{H.G_2}$ suggest an efficient FRET based process involving the donor pyrene fragment and the acceptor coumarin unit. Control experiments in CH_2Cl_2 solution having an equimolar mixture of **H** and unsubstituted coumarin

DOI: 10.1021/acs.joc.6b01631
J. Org. Chem. 2016, 81, 8977−8987

imidazolium guest were performed using λ_{ext} of 314 nm, and no such increase in coumarin based emission was observed (Figure S12). The excitation spectra recorded for the equimolar mixture of **H** and $\mathbf{G_1}$ (solution having predominantly $\mathbf{H{:}G_1}$ using λ_{mon} of 378 nm) or $\mathbf{G_2}$ (solution having predominantly $\mathbf{H{:}G_2}$ using λ_{mon} of 400 nm) revealed the pattern for the absorption spectrum of the respective donor moiety (Figure S10). These further corroborated our presumption for a FRET based energy transfer pathway.

Time Resolved Emission Studies. Time correlated single photon counting (TCSPC) studies were performed for individual components as well as for the host–guest assembly in the CH_2Cl_2 solution for developing a better insight about the FRET processes. The fluorescence lifetimes of the individual components (**H**, $\mathbf{G_1}$, and $\mathbf{G_2}$) and corresponding host–guest adducts ($\mathbf{H.G_1}$ and $\mathbf{H.G_2}$) are provided in Table 1.

Table 1. Summary of Time Resolved Lifetime Details[a]

system	λ_{ext} (nm)	λ_{mon} (nm)	τ (ns)
H	310	378	$\tau_1 = 6.3 \pm 0.01$ (12.75%); $\tau_2 = 28.54 \pm 0.003$ (87.25%)
$\mathbf{G_1}$	295	340	$\tau_1 = 4.7 \pm 0.08$ (18.28%); $\tau_2 = 10.54 \pm 0.04$ (81.72%)
$\mathbf{G_2}$	340	410	$\tau_1 = 0.596 \pm 0.007$ (86.84%); $\tau_2 = 4.46 \pm 0.04$ (13.16%)
$\mathbf{H + G_1}$	295	378	$\tau_1 = 6.4 \pm 0.1$ (8.09%); $\tau_2 = 30.0 \pm 0.04$ (91.91%)
$\mathbf{H + G_2}$	310	410	$\tau_1 = 1.35 \pm 0.08$ (66.32%); $\tau_2 = 21.54 \pm 0.05$ (33.68%)

[a]Measurements are done in dichloromethane. In the case of $\mathbf{H + G_1}$/$\mathbf{G_2}$ (1:1) molar mixtures are used, and for all measurements $1 \leq \chi^2 \leq 1.2$.

On excitation at 295 nm (LED) a biexponential decay profile was observed for $\mathbf{G_1}$, $\tau_1 = 4.7 \pm 0.08$ ns (18.3%) and $\tau_2 = 10.54 \pm 0.04$ ns (81.7%). The 10.54 ns component was anticipated for the naphthalene moiety. A similar biexponential decay profile was also observed for **H**, $\tau_1 = 6.29 \pm 0.01$ ns (12.75%) and $\tau_2 = 28.54 \pm 0.003$ ns (87.25%). Emission decay profile for 1:1 mixture of **H** and $\mathbf{G_1}$ was monitored at 340 nm following excitation at 295 nm (λ_{max} for naphthalene moiety) (Figure S13). Data presented in Table 1 clearly reveal that, on predominant excitation of the donor (naphthalene) moiety, there is a distinct decrease in the donor component with a substantial increase in the component for the acceptor lifetime in the overall emission decay profile. This further supports the FRET based ET from naphthalene moiety to pyrene moiety in the host–guest adduct ($\mathbf{H.G_1}$). We failed to resolve if there had been any rise time component in the overall decay profile for $\mathbf{H.G_1}$, which could be due to a much faster ET transfer than the fluorescent decays of both the donor and the acceptor. Energy transfer efficiency was evaluated to be 52.25%, while Förster distance (R_o) was evaluated as 30.2 Å for $\mathbf{H.G_1}$ in dicholoromethane solution. Similar studies were also performed with a solution of $\mathbf{G_2}$, and data were compared with that recorded for an equimolar mixture of **H** and $\mathbf{G_2}$ in CH_2Cl_2 medium (λ_{ext} = 310 nm; λ_{mon} = 410 nm) (Table 1). On excitation at 310 nm (pyrene absorbs predominanty) for equimolar mixture $\mathbf{H.G_2}$ solution, a substantial decrease in the donor (pyrene) component with subsequent increase in the acceptor (coumarin) component was observed for λ_{mon} at 410 nm (Figure S14). Based on the time-resolved emission data, energy transfer efficiency and Förster distance (R_o) were evaluated as 69.37% and 14.12 Å, respectively. Data derived from the emission decay profile also enabled us to evaluate the ET rates, which were found to be 1.2×10^8 s^{-1} for $\mathbf{H.G_1}$ and 8.81×10^7 s^{-1} for $\mathbf{H.G_2}$. FRET based energy transfer for the host–guest adducts ($\mathbf{H.G_1}$ and $\mathbf{H.G_2}$) ensures that donor and acceptor fluorophores are within the interacting distances with favorable transitional dipole moments for respective donor/acceptor fluorophore. Also, the interchromophoric distance between naphthalene and pyrene in $\mathbf{H{:}G_1}$ complex is evaluated as 30.10 Å, whereas this distance between pyrene and coumarin moieties is evaluated as 12.33 Å for $\mathbf{H{:}G_2}$ complex in dichloromethane solution. Considering the fact that the FRET mechanism is effective only when the interchromophoric distances are within 10–100 Å), our results clearly suggest that two chromophoric pairs, namely, naphthalene–pyrene in $\mathbf{H.G_1}$ and pyrene–coumarinin $\mathbf{H.G_2}$, are favorably placed for FRET based mechanism to prevail.

NMR Studies. The complexation of aza crown based host (**H**) with two different imidazolium based guest molecules ($\mathbf{G_1}$ and $\mathbf{G_2}$) in CD_2Cl_2 were studied in detail using ^1H NMR spectroscopic studies. It is well documented that derivatives of imidazolium ion or its derivatives form inclusion complexes ($K_a \sim 10^3$ M^{-1} in acetonitrile medium at 25 °C) with DB24CO8 or its derivatives as host molecules via H-bonding.[8,19a,b] In our earlier studies we have established that NO_6 based aza-crown ether derivative, specifically **H**, formed stable inclusion complexes with secondary ammonium ion.[12a] It is also well documented that, in dilute solution, imidazolium salts exist as highly dissociated naked ions.[8,19] In 1,3-disubstituted imidazolium salts, all protons on the imidazolium ring are quite acidic due to an effective delocalization of the positive charge over the entire imidazolium ring. These acidic hydrogen atoms also participate in H-bond $[(C{-}H)_{imidazolium}{\cdots}O_{crown}]$ formation involving the lone pair of electrons of the oxygen/nitrogen atoms on the aza-crown moiety, and this accounts for the stability of the adduct formed.

Let us first discuss the results of ^1H NMR spectral studies involving **H** and $\mathbf{G_1}$. ^1H NMR spectra of $\mathbf{G_1}$ (5.27×10^{-3} M) were recorded in CD_2Cl_2 in the absence and presence of varying concentration of **H** (0–15.07×10^{-3} M). At room temperature, only one set of signal was observed in the ^1H NMR spectrum of the solution having equimolar amounts of **H** and $\mathbf{G_1}$ (Figure 3C), which implied that the equilibrium kinetics were fast and rapid exchange between complexed and uncomplexed species happened within the NMR time scale. No further change was observed when additional **H** was added (even for $[\mathbf{H}]{:}[\mathbf{G_1}] \geq 1{:}2$). This confirmed that the equilibrium was achieved at these concentrations for **H** and $\mathbf{G_1}$. For **H**, majority protons show downfield shifts ($\Delta\delta_{H_{a,b}}$ = 0.21 ppm, $\Delta\delta_{H_c}$ = 0.18 ppm, $\Delta\delta_{Hd}$ = 0.15 ppm, $\Delta\delta_{He}$ = 0.18 ppm, $\Delta\delta_{Hg}$ = 0.20 ppm, $\Delta\delta_{Hf}$ = 0.14 ppm, and $\Delta\delta_{Hh}$ = 0.27 ppm) on formation of the adduct $\mathbf{H.G_1}$. In the case of $\mathbf{G_1}$, the signal for the H_8 proton experiences a marginal upfield shift ($\Delta\delta_{H8}$ = −0.01) in $\mathbf{H.G_1}$ compared to free compound $\mathbf{G_1}$. Relatively higher downfield shifts are evident for H_h and H_g, these support H-bond/electrostatic interaction between the lone pair of electrons of N_{amine} [H] and the imidazolium ion on adduct ($\mathbf{H.G_1}$) formation. Presumably, H_8 proton lies little in the shielded environment due to its proximity and the ring current of the pyrene ring in **H**. H_2 proton of the imidazolium moiety is acidic and expected to be downfielded shifted on formation of

DOI: 10.1021/acs.joc.6b01631
J. Org. Chem. 2016, 81, 8977–8987

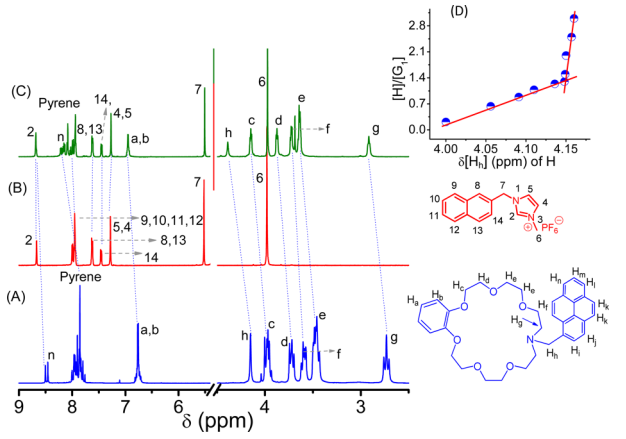

Figure 3. Partial ^{1}H NMR spectra of (A) 5.27 × 10^{-3} M **H**, (B) 5.27 × 10^{-3} M $\mathbf{G_1}$, and (C) an equimolar mixture of **H** and $\mathbf{G_1}$ in CD_2Cl_2 (500 MHz) and (D) mole ratio plot for the complexation of **H** with $\mathbf{G_1}$ using $\Delta\delta$ (ppm) for the H_h proton in **H**.

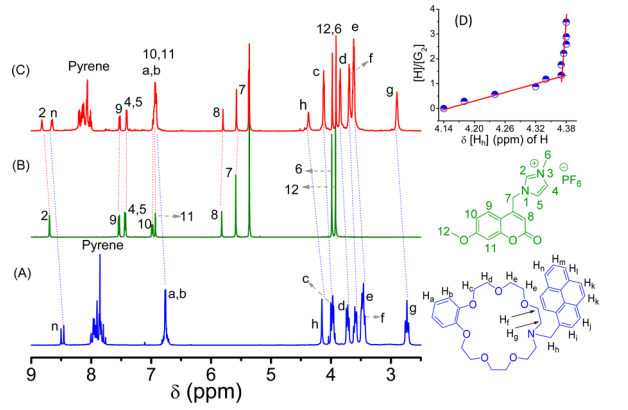

Figure 4. Partial ^{1}H NMR spectra of (A) 4.42 × 10^{-3} M **H**, (B) 4.42 × 10^{-3} M $\mathbf{G_2}$, and (C) an equimolar mixture of **H** and $\mathbf{G_2}$ in CD_2Cl_2 (500 MHz) and (D) mole ratio plot for the complexation of **H** with $\mathbf{G_2}$ using $\Delta\delta$ (ppm) for the H_h proton in **H**.

$(H_2)_{imidazolium}\cdots O/N_{crown}$ H-bonding. As anticipated, a downfield shift of 0.03 ppm for H_2 proton is observed. Relatively smaller shift is presumably due to a weak H-bond interaction. Similarly, a weak H-bond interaction is also observed for H_7 ($\Delta\delta_{H7}$ = 0.03) proton. Most other naphthalene ring protons in $\mathbf{H.G_1}$ have appeared in the same region where most pyrene protons have appeared, and thus, it is difficult to assign the shift for any such individual protons. Little but definite upfield shifts are observed for H_9 ($\Delta\delta$ = −0.04) and H_{14} ($\Delta\delta$ = −0.02) protons. All these tend to suggest a weak but certain $\pi-\pi$ stacking interaction involving $\mathbf{H}_{pyrene}$ moiety and $\mathbf{G}_{naphthalene}$ moieties. This also suggests the favorable orientation of the fluorophores for the FRET based energy transfer process. Downfield shifts for H_2 proton suggest the formation of a threaded complex for $\mathbf{H.G_1}$. Nonetheless, ^{1}H NMR studies enabled us to understand the relative orientation of the guest molecule ($\mathbf{G_1}$) in $\mathbf{H.G_1}$ adduct.

As the most prominent shift is observed for H_h of the host (**H**), systematic changes in the $\Delta\delta_{Hh}$ are plotted as a function of varying [**H**]:[$\mathbf{G_1}$] with systematic changes in [**H**] (Figure 3D). A clear breakpoint appears at [**H**]:[$\mathbf{G_1}$] = 1.31, which further suggests an adduct formation with 1:1 stoichiometry. This helped us also in evaluating the formation constant as (1.82 ± 0.03) × 10^3 M^{-1} by analyzing the sequential changes in chemical shift value of H_h at various concentrations of **H**, which reveals its moderate affinity toward imidazolium ions.

Systematic ^{1}H NMR titrations were also carried out for another guest, $\mathbf{G_2}$. As observed for $\mathbf{G_1}$, only one set of proton NMR signals is observed (Figure 4C), and this confirms a fast exchange process within the NMR time scale. Most prominent down field shifts are observed for H_h ($\Delta\delta_{Hh}$ = 0.22 ppm) and H_g ($\Delta\delta_{Hg}$ = 0.17 ppm). Ethylene glycol chain protons show a little downfield shift in the presence of $\mathbf{G_2}$: $\Delta\delta_{H_c}$ = 0.15 ppm, $\Delta\delta_{Hd}$ = 0.10 ppm, $\Delta\delta_{He}$ = 0.16 ppm, $\Delta\delta_{Hf}$ = 0.12 ppm, $\Delta\delta_{Hg}$ = 0.17 ppm, and $\Delta\delta_{Hh}$ = 0.24 ppm. As anticipated, a downfield shift ($\Delta\delta_{H2}$ = 0.12 ppm) is observed also for H_2, which confirms H-bonding interaction between O_{crown} and acidic H_2 proton on imidazolium ring. Appreciable downfield shift is observed for H_n ($\Delta\delta_{Hn}$ = 0.20 ppm) and $H_{a,b}$ ($\Delta\delta_{H_{a,b}}$ = 0.18 ppm) protons. Binding stoichiometry of 1:1 is evaluated from the plot of systematic changes in the $\Delta\delta_{Hh}$ with changes in [**H**]:[$\mathbf{G_2}$] with systematic changes in [$\mathbf{G_2}$] (Figure 4D). Using this binding stoichiometry, the formation constant for $\mathbf{H.G_2}$ is evaluated as (1.17 ± 0.03) × 10^3 M^{-1} from the Benesi–Hildebrand (B–H) plot (Figure S15). Changes for all other protons for **H** and $\mathbf{G_2}$ in $\mathbf{H.G_2}$ are almost similar as observed in the case of $\mathbf{H.G_1}$. This justifies almost similar formation constant for two respective inclusion complexes, $\mathbf{H.G_1}$ and $\mathbf{H.G_2}$.

To gain insight into the molecular interactions and the spatial orientations of the individual components in the host–guest assembly, we performed 2D NMR studies. NOESY experiments are generally well suited for this purpose, even though the COSY peaks are more intense at the concentrations used (Figure S16). In the NOESY spectrum recorded for an equimolar mixture of **H** and $\mathbf{G_1}$, the spatial distance between interacting protons must be less than 5 Å to observe cross peaks. The NOESY spectrum of an equimolar mixture of **H** and $\mathbf{G_1}$ in CD_2Cl_2 gave intense cross peaks between the H_7 proton of $\mathbf{G_1}$ and the pyrene protons of **H** (Figure 5A). These cross peaks are evidence for the inclusion complex between **H** and $\mathbf{G_1}$.

Moreover, the presence of cross peaks of $H_{9,10,11,12}$ of $\mathbf{G_1}$ with H_g of **H**(ethylenoxy protons) clearly shows the interactions between $\mathbf{G_1}$ and **H**. A strong correlation is observed between the $H_{9,10,11,12}$ protons of $\mathbf{G_1}$ with H_h of **H**. Weak cross peaks are also observed between $H_{9,10,11,12}$ of $\mathbf{G_1}$ and certain protons ($H_{e,f}$) of the crown ether moiety. These data clearly establish the formation of a threaded complex for the host–guest adduct $\mathbf{H.G_1}$.

The NOESY spectrum of an equimolar mixture of **H** and $\mathbf{G_2}$ also shows intense cross peaks between $H_{a,b}$ of **H** and $H_{6,12}$ of the imidazolium residue of $\mathbf{G_2}$. Cross peaks are also observed between $H_{10,11}$ of the imidazolium residue and the H_c protons of the **H** (Figure 5B). This observation can be interpreted as a spatial proximity of the crown ether cavity with the imidazolium residue (Scheme 1).

Results of the ESI mass spectral studies also confirm the binding stoichiometry of 1:1. The mass spectrum recorded for **H** and $\mathbf{G_1}$ (with [**H**]:[$\mathbf{G_1}$] is 1:2) showed a signal for m/z of 791, which could be attributed to ($\mathbf{H} + \mathbf{G_1} - PF_6^+$) (Figure S17), while that for **H** and $\mathbf{G_2}$ appeared at 985 for ($\mathbf{H} + \mathbf{G_2} + H^+$) (Figure S18). Thus, mass spectral data also corroborate our findings of fluorescence and ^{1}H NMR spectral studies.

Electrochemical Studies. In order to check the thermodynamic feasibility of the FRET process, HOMO and

DOI: 10.1021/acs.joc.6b01631
J. Org. Chem. 2016, 81, 8977–8987

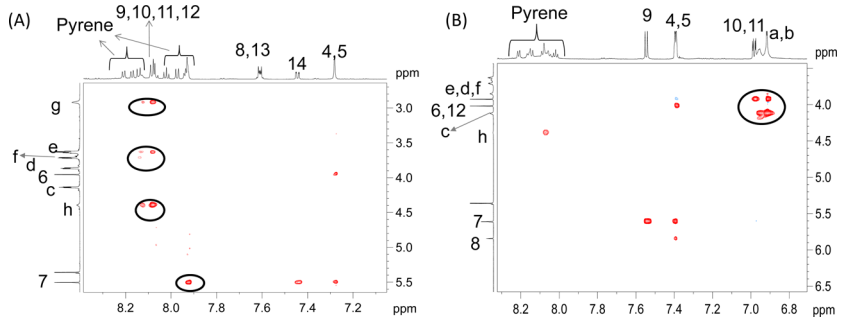

Figure 5. Correlation of the aromatic protons of imidazolium units with the ethylenoxy protons of the **H** unit in the NOESY spectrum in CD_2Cl_2 with (A) $\mathbf{G_1}$ and (B) $\mathbf{G_2}$.

Scheme 1. Proposed Molecular Structure for H.G_1 and H.G_2 with Spatial Proximity between Two FRET Pairs, Namely, Naphthalene−Pyrene and Pyrene−Coumarin in H.G_1 and H.G_2, Respectively

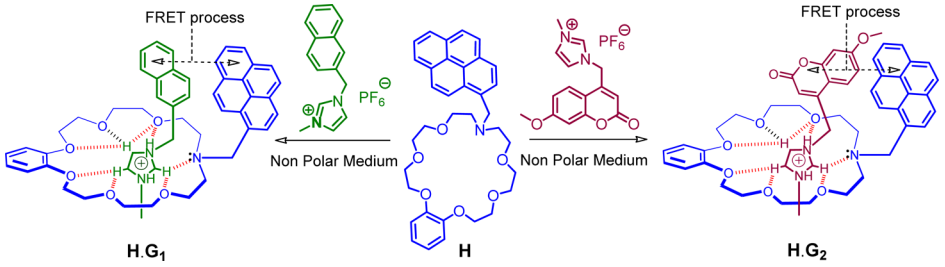

LUMO energy levels of respective fluorophores were evaluated from the data available from electrochemical studies as well as the information derived from absorption/emission spectra. The intersection of the absorption and emission spectra for each fluorophore in **H**, $\mathbf{G_1}$, and $\mathbf{G_2}$ was used for calculating the ΔE_{0-0} value for the respective fluorophore. Oxidation potential data for **H**, $\mathbf{G_1}$, and $\mathbf{G_2}$ were evaluated from electrochemical studies of respective species, and these are linked to HOMO levels of the acceptor fluorophores.

Oxidation potential for $\mathbf{G_1}$, **H**, and $\mathbf{G_2}$ are found to be 1.56, 1.34, and 1.634 V, respectively (Figure S19). The E_{0-0} value for three respective chromophores could be used for evaluating the HOMO−LUMO energy gap and these values, 3.92 ($\mathbf{G_1}$), 3.42 (**H**), and 3.28 ($\mathbf{G_2}$) eV (Figure 6). Subsequently, the HOMO−LUMO energy gap and E_{0-0} value for the respective luminophore are used for estimating the LUMO energy for the three chromophores (Figure 6). These values clearly confirm the thermodynamic feasibility of the energy transfer process involving naphthalene as donor and pyrene as acceptor in H.G_1 and pyrene as donor and coumarin as acceptor in H.G_2.

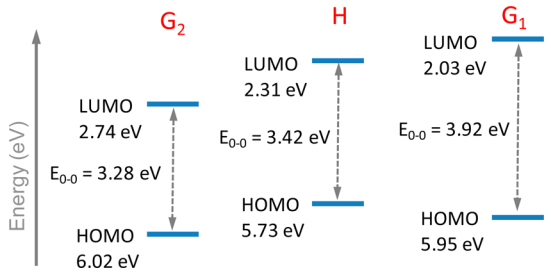

Figure 6. Schematic representation of the HOMO−LUMO energy levels for $\mathbf{G_1}$, **H**, and $\mathbf{G_2}$, which confirm the feasibility of energy transfer between naphthalene$_{G_1}$ → pyrene$_H$ and pyrene$_H$ → coumarin$_{G_2}$.

Isothermal Titration Calorimetry Studies. Binding constants and thermodynamic data for the inclusion complex formation were evaluated from ITC studies. In a typical ITC experiment, a solution of the host (**H**) is placed in the sample cell and is treated stepwise with small amounts of a solution of the guest $\mathbf{G_1}$ or $\mathbf{G_2}$. The titrations were performed at 298 K in CH_2Cl_2 (Figure 7). Experimental data confirmed formation of 1:1 binding stoichiometry for both complexes. A control experiment was carried out in each run to determine the heat of dilution by injecting a solution of host or guest into CH_2Cl_2 containing no guest or host molecules, respectively. The heat of dilution evaluated in the control experiment was subtracted

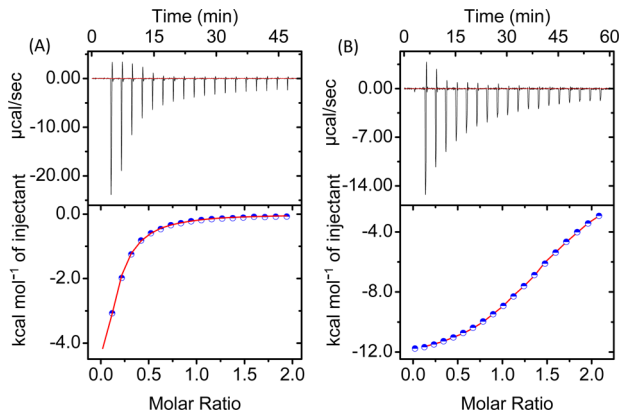

Figure 7. ITC titration profiles for the inclusion complex formation between (A) **H** (5 mM) and $\mathbf{G_1}$ (51.08 mM) and (B) **H** (7 mM) and $\mathbf{G_2}$ (71.09 mM) in dichloromethane (298 K). Raw data for the sequential injection of the $\mathbf{G_1}$ and $\mathbf{G_2}$ into host in steps of 2 μL is shown in the top panel. Heat evolutions on addition of the guests into host are shown in the bottom panel.

DOI: 10.1021/acs.joc.6b01631
J. Org. Chem. 2016, 81, 8977−8987

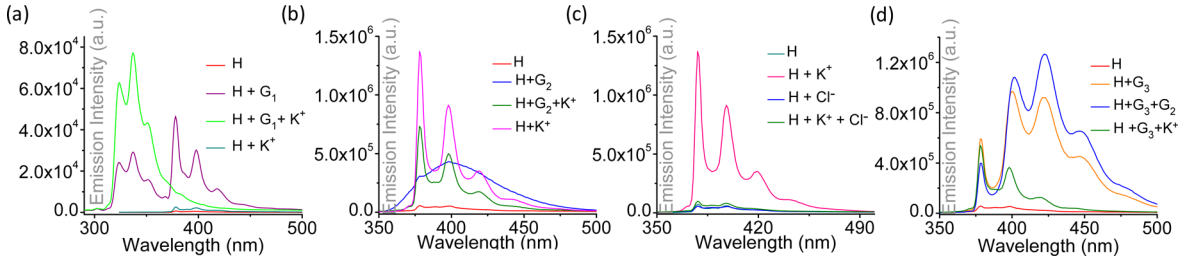

Figure 8. Fluorescence spectral responses recorded in CH_2Cl_2 at 25 °C for **H** with (a) $\mathbf{G_1}$, $\mathbf{G_1}$ + KPF_6, and KPF_6; (b) $\mathbf{G_2}$, $\mathbf{G_2}$ + KPF_6, and KPF_6; (c) KPF_6, Cl^-, and Cl^- + KPF_6, and (d) $\mathbf{G_3}$, $\mathbf{G_3}$ + $\mathbf{G_2}$, and $\mathbf{G_3}$ + KPF_6. λ_{ext} used are (a) 277 nm, (b) 314 nm, (c) 314 nm, and (d) 314 nm, respectively.

from the apparent heat of the reaction measured in the titration experiments for calculating the net reaction heat. As anticipated, the heat of reaction was found to decrease after each injection of the host molecules. The binding constants for the formation of $\mathbf{H.G_1}$ and $\mathbf{H.G_2}$ were evaluated as (2.61 ± 0.015) × 10^3 M^{-1} ($K_{\mathbf{H\cdot G_1}}$) and (1.27 ± 0.16) × 10^3 M^{-1} ($K_{\mathbf{H\cdot G_2}}$), respectively.

Binding processes were governed by negative enthalpy changes: ΔH° = −14.48 ± 0.032 kcal mol^{-1} for $\mathbf{H.G_1}$ and ΔH° = −12.91 ± 0.059 kcal mol^{-1} for$\mathbf{H.G_2}$. Associated entropy changes were also observed ($T\Delta S$ = −10.22 kcal/mol for $\mathbf{H.G_1}$, $T\Delta S$ = −7.92 kcal/mol for $\mathbf{H.G_2}$). Calculated binding free energies are −4.258 kcal mol^{-1} and −4.983 kcal mol^{-1} for $\mathbf{H.G_1}$ and $\mathbf{H.G_2}$, respectively. It is well-known that the association process arising from conformational freedom and the desolvation effect is entropically favored ($T\Delta S$ < 0), whereas, the negative enthalpy contributions (ΔH < 0) arise mainly from the electrostatic, hydrogen-bonding, $\pi-\pi$, and van der Waals interactions upon complexation.[20] Binding constants that were evaluated from ITC experiments for $\mathbf{H.G_1}$ and $\mathbf{H.G_2}$ followed a similar trend that was observed for data evaluated from ^{1}H NMR titration data in CD_2Cl_2. The ^{1}H NMR titration data gave a relatively low binding constant value, compared to the value obtained from ITC measurements.

Self-Sorting Phenomena. Nature efficiently uses the principle of self-sorting phenomena to generate complex functional architectures.[21] In the past decades, this has been used effectively for achieving a varieties of supramolecular systems and the self-organization of nanostructures.[21a,d,22a] Various factors such as recognition motifs, size, shape, thermodynamic and kinetic binding parameters, and stoichiometry are responsible for self-discrimination.[22,16a,21c] It is well documented that K^+ forms strong complexes with crown ether and its derivatives.[23] The binding constant for $\mathbf{H.K^+}$ ($K_{\mathbf{H.K^+}}$ = (7.2 ± 0.07) × 10^4 M^{-1}) was evaluated by fluorescence titration, and this was higher by an order of magnitude compared to those for $\mathbf{H.G_1}$ and $\mathbf{H.G_2}$. Taking advantage of the differences in the binding affinities of $\mathbf{G_1}$/$\mathbf{G_2}$ and K^+ toward **H**, the higher binding affinity of K^+ toward C18O6 (K_a = 1.3 × 10^6 M^{-1} in methanol at 25 °C)[23a] as compared to **H** (*vide infra*), and reversible formation of host−guest complexes, associated luminescence responses could be correlated for demonstrating the Boolean operations.[13] The emission spectrum of **H** was recorded in the presence of K^+ and K^+ + C18O6 or Cl^- (in given sequence) following excitation at 314 nm (λ_{ext}^{pyrene}). Spectra recorded for **H** in the presence of K^+ showed strong pyrene based emission on formation of K^+**H**, as coordination to K^+ would have interrupted the PET process. Spectra recorded on further addition of C18O6 or Cl^- to the solution of K^+**H** showed complete quenching of the pyrene based luminescence. This was understandable, as both C18O6 and Cl^- were expected to bind preferentially to K^+ and caused complete decomplexation with simultaneous generation of free **H** (Figures S20, S21).

As discussed earlier, $\mathbf{H.G_1}$ (1:2 molar equiv) solution on excitation at 277 nm (predominantly naphthalene-based excitation) shows a FRET based fluorescence response that is characteristic for the pyrene moiety of **H** (Figure 8a). Binding affinity of K^+ toward **H** is much higher as compared to $\mathbf{G_1}$, and this led to the dethreading of $\mathbf{H.G_1}$ with concomitant formation of $\mathbf{HK^+}$ and free **H**. This results in a complete quenching of the pyrene based emission (Figure 8a), which is understandable if we consider that $\mathbf{HK^+}$ has insignificant absorbance at 277 nm. Identical emission responses were anticipated and observed when K^+ was added to the solution of $\mathbf{H.G_2}$, as this also led to the formation of $\mathbf{HK^+}$ and free $\mathbf{G_2}$ (Figure 8b). For both these instances, pyrene based emission could only be observed when 314 nm (λ_{ext}^{pyrene}) was used as excitation wavelength (Figure 8b).

Earlier discussions (*vide infra*) have established that K^+ has a higher affinity toward C18O6 as compared to that for **H**. A solution having **H** + $\mathbf{G_1}$ + K^+ showed an emission spectrum that is characteristic for $\mathbf{G_1}$; a typical naphthalene based emission as λ_{ext} of 277 nm ($\lambda_{ext}^{naphthalene}$) was used as excitation wavelength. However, on addition of C18O6, formation of C18O6-K^+ prevailed, and this led to generation of free **H** for $\mathbf{G_1}$ to form a threaded complex $\mathbf{H.G_1}$ with a FRET based emission response that is characteristic for pyrene moiety for λ_{ext} of 277 nm. This fluorescence response clearly helped in demonstrating the self-sorting phenomenon. Similar observation was also observed when Cl^- was used instead of C18O6, as Cl^- formed a tight ion pair with K^+ and this led to the decomplexation of the K^+ from K^+**H** with complete quenching of pyrene based emission (λ_{ext} of 277 nm; Figure 8c). ESI mass spectra obtained for a 1:1:1 mixture of **H**, $\mathbf{G_1}$ or $\mathbf{G_2}$, and K^+ showed *m*/*z* signal at 608, which signified the formation of $\mathbf{HK^+}$ and clarified that K^+ could actually replace $\mathbf{G_1}$ or $\mathbf{G_2}$ from the complexes $\mathbf{H.G_1}$ and $\mathbf{H.G_2}$, respectively (Figure S22 and S23).

For further demonstration of the self-sorting phenomenon, the binding process with another guest molecule ($\mathbf{G_3}$) is utilized. Earlier studies reveal that secondary ammonium ion derivative forms a stronger inclusion complex than the imidazolium ion with NO_6 based aza-crown ether.[12a] Accordingly, we have utilized a previously reported guest molecule $\mathbf{G_3}$ (as hexafluoro phosphate salt).[12a] The absorption spectrum of anthracene has a strong spectral overlap with the emission spectrum of pyrene, and this is the primary reason for choosing anthracene as the fluorophore in $\mathbf{G_3}$. To take the advantage of the higher binding affinity of $\mathbf{G_3}$ toward **H**, $\mathbf{G_3}$ was added to a solution that predominantly had $\mathbf{H.G_2}$ in equilibrium. By virtue of its higher affinity, $\mathbf{G_3}$ replaced $\mathbf{G_2}$

DOI: 10.1021/acs.joc.6b01631
J. Org. Chem. 2016, 81, 8977−8987

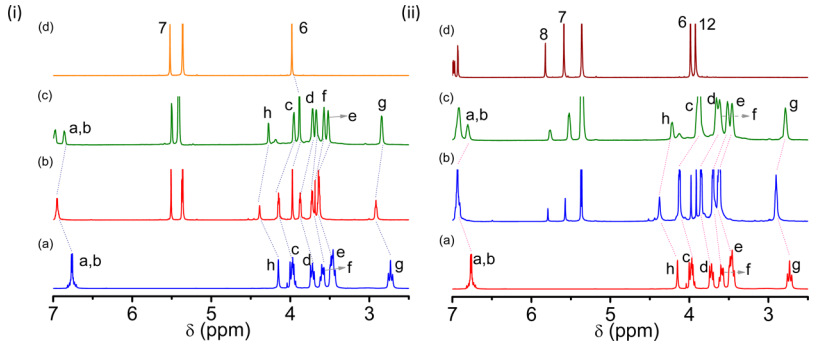

Figure 9. Partial ^{1}H NMR spectra (500 MHz, 298 K) recorded in 4:1 (v/v) CD_2Cl_2:CD_3CN for (i) (a) 3.5 mM **H**, (b) 3.5 mM **H** with 3.5 mM $\mathbf{G_1}$, (c) 3.5 mM **H** with 3.5 mM $\mathbf{G_1}$ and then 3.5 mM KPF_6, and (d) 3.5 mM $\mathbf{G_1}$ and (ii) (a) 2.7 mM **H**, (b) 2.7 mM **H** with 2.7 mM $\mathbf{G_2}$, (c) 2.7 mM **H** with 2.7 mM $\mathbf{G_2}$ and then 2.7 mM KPF_6, and (d) 2.7 mM $\mathbf{G_2}$.

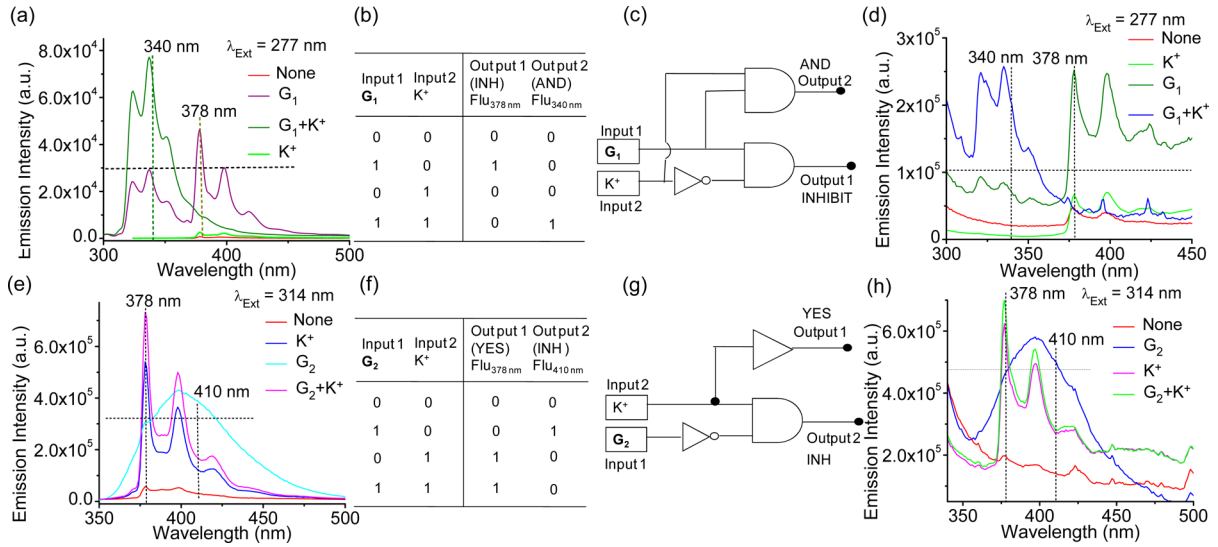

Figure 10. Fluorescence spectra of **H** under different input conditions in the solution state and then treated with (a) $\mathbf{G_1}$ and K^+ and (e) $\mathbf{G_2}$ and K^+; in the solid state using silica surface and then treated with (d) $\mathbf{G_1}$ and K^+ and (h) $\mathbf{G_2}$ and K^+. The truth table corresponds to the inputs (b) $\mathbf{G_1}$ and K^+ and (f) $\mathbf{G_2}$ and K^+. In this study, (a) [**H**] = 7.75×10^{-7} M and (e) [**H**] = 1.68×10^{-5} M were used; **H**:$\mathbf{G_1}$ = 1:1, **H**:K^+ = 1:1, and **H**:$\mathbf{G_1}$:K^+ = 1:1:1 molar ratio were used. The combinatorial logic schemes are shown in (c) $\mathbf{G_1}$ and K^+ and (g) $\mathbf{G_2}$ and K^+. The horizontal dashed line marks the threshold value. λ_{ext} was used for (a) 277 nm and (d) 314 nm.

from $\mathbf{H.G_2}$, and on excitation at 314 nm (λ_{ext}^{pyrene}), a distinct anthracene based emission was observed (Figure 8d). This was attributed to the formation of the threaded complex $\mathbf{H.G_3}$ with associated FRET based response from the anthracene fragment (Figure 8d).[12a] Further on addition of KPF_6 to this CH_2Cl_2 solution, $\mathbf{H}K^+$ was formed with subsequent generation of free $\mathbf{G_3}$, and this accounted for only pyrene based emission on excitation at 314 nm. However, the process was reversed on subsequent addition of C18O6. As mentioned above, 18-crown-6 does not interact with $\mathbf{G_1}$/$\mathbf{G_2}$/$\mathbf{G_3}$, but forms a strong complex with the K^+ and helps **H** to form a threaded complex ($\mathbf{H.G_3}$) with $\mathbf{G_3}$ (Figure 8d). These results clearly revealed that the formation of the crown ether based pseudorotaxanes can be switched *off* and *on* in a controllable manner simply by utilizing the differences in affinities of different guests toward different host molecules.

Results of the ^{1}H NMR studies also demonstrated this self-sorting process. When one mole equivalent of KPF_6 was added to a solution having one mole equivalent of **H** + $\mathbf{G_1}$ in CD_2Cl_2, a distinct reversible change in the ^{1}H NMR spectrum was observed. In the presence of K^+, $\mathbf{H.G_1}$ dissociated and formation of $\mathbf{H}K^+$ prevailed, and these were evident in the ^{1}H NMR spectral changes (Figure 9i). The spectral shifts induced by the complexation of **H** and $\mathbf{G_1}$ disappeared on formation of $\mathbf{H}K^+$. Analogous changes were also observed when similar studies were repeated for $\mathbf{G_2}$ (Figure 9ii). All these data confirmed that K^+ can actually replace the imidazolium-based guests from the host (**H**) cavity.

Photophysical Properties in Film and Construction of Logic Gates. Demonstration of optical responses on solid surface is preferred for developing any optoelectronic devices. To explore such a possibility, modified silica films were obtained by drop casting host/guest/K^+solution ([**H**] = 1.68×10^{-6} M in CH_2Cl_2 solution and equimolar amount of other inputs were used for studies) onto silica plates (layer thickness 0.2 mm) and air-dried at 35 °C prior to our use. Initially, spectra were recorded (λ_{ext} of 277 nm) for silica surface modified with only **H**. Then, these plates were exposed to different sets of guest/host and/or K^+ ions and luminescence spectra were recorded accordingly (Figure S24–S26). The primary objective was to demonstrate the logic operation by monitoring the emission responses of **H** in the presence of different inputs on solid surface during a reversible supramolecular assembly formation.

DOI: 10.1021/acs.joc.6b01631
J. Org. Chem. 2016, 81, 8977–8987

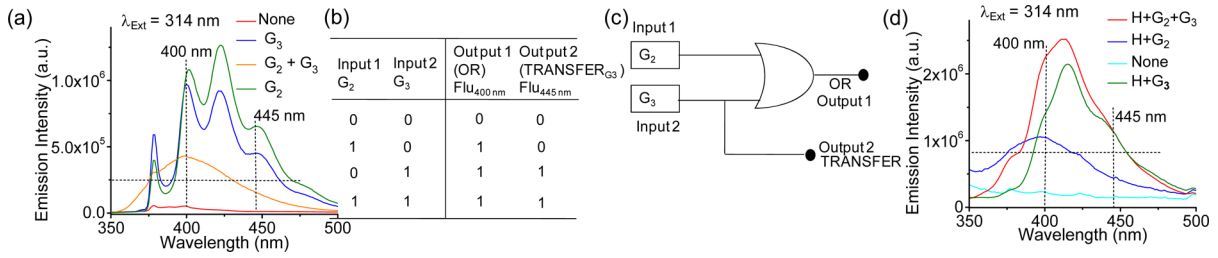

Figure 11. Fluorescence spectral response of **H** with different input added in sequence (a) in solution with $\mathbf{G_2}$ and $\mathbf{G_3}$ and (d) on silica surface with $\mathbf{G_2}$ and $\mathbf{G_3}$. (b) The truth table corresponds to the input $\mathbf{G_2}$ and $\mathbf{G_3}$ in sequence and (c) the combinatorial logic scheme for inputs $\mathbf{G_2}$ and $\mathbf{G_3}$. The horizontal line marks the threshold value for emission intensity. For this study [**H**] of 1.68×10^{-5} M, $\mathbf{H{:}G_3}$ = 1:1.1 molar equiv, $\mathbf{H{:}G_2}$ 1:1 molar ratio, and $\mathbf{H{:}G_2{:}G_3}$ 1:1:1 molar ratio were used.

The possibility of reconfiguring the optical output of the photoactive molecules in the presence of certain molecular or ionic inputs has special relevance for developing molecular logic gates. We have taken the advantages of the difference on the relative affinities of $\mathbf{G_1}/\mathbf{G_2}$ and $\mathbf{G_3}$ or K^+ toward **H**, as well as the preferential binding of K^+ to C18O6 as compared to **H** for achieving different luminescence responses. Interestingly, such luminescence responses in the presence of various ionic ($\mathbf{G_1}$, $\mathbf{G_2}$, $\mathbf{G_3}$, K^+ used either alone or in different combinations) inputs, either in solution or on a silica based thin film of the host (**H**), could be correlated for demonstrating Boolean operations.

By taking appropriate threshold values and a logic convention, the molecular/ionic input and output emission signals could be used to encode binary information. For demonstrating this, emission intensities were monitored at 340 and 378 nm (λ_{ext} = 277 nm) using a threshold emission intensity value of 3.0×10^4. Emission intensities above and below this threshold value are considered as "1" and "0", respectively. In the absence of any ionic input ($\mathbf{G_1}$, input 1,or K^+, input 2), output is "0", be it monitored at 378 or 340 nm (Figure 10).

First, we examined the luminescence responses of **H** either in solution or on silica surface in the absence/presence of either one or both of the ionic inputs ($\mathbf{G_1}$ and K^+; Figures 10a–d). Threshold values for emission intensities were used as 3.0×10^4 and 1.0×10^5 for studies with solution and silica surface, respectively. In the presence of inputs (1,0), outputs at 378 and 340 nm are "1" and "0", respectively. In the presence of inputs (0,1), outputs are "0" and "0", respectively, at 378 and 340 nm. In the presence of both inputs (1,1), formation of $\mathbf{HK^+}$ would prevail in solution, which accounted for outputs "0" and "1" at 378 and 340 nm, respectively. Thus, an active output "1" is obtained at 378 nm only when $\mathbf{G_1}$ (1,0) is present as input (truth table in Figure 10b), and this could be correlated to inhibit (INH) logic function, as output is "1" obtained only when one particular input ($\mathbf{G_1}$) is present (1). Luminescence response at 340 nm could be correlated to an "AND" (Figure 10a) logic operation, as an output signal "1" is achievable only when two inputs (1,1) are present.[13]

Next we examined the luminescence responses of **H** either in solution or on silica surface in the absence/presence of either one or both of the ionic inputs $\mathbf{G_2}$ and K^+ (Figures 10e–h) following excitation at 314 nm and using threshold intensity value of 3.2×10^5 and 4.75×10^5 for solution and solid surface, respectively. Emission responses below ("0") and above ("1") this threshold value in the absence/presence of ionic inputs like $\mathbf{G_2}$ and K^+ are summarized in the truth table (Figure 10f). For the monitoring wavelength of 410 nm, output 2 responses could be correlated to an INH logic operator, while for fluorescence responses monitored at 378 nm, output 1 responses were found to be consistent with a YES logic operator. The YES gate transforms one input signal to output neglecting another input signal.

Taking advantage of the preferential binding of **H** with $\mathbf{G_3}$ even in the presence of another guest molecule like $\mathbf{G_2}$, luminescence responses could be correlated for demonstrating a more complicated logic operation. For this, $\mathbf{G_2}$ (input 1) and $\mathbf{G_3}$ (input 2) were used as two ionic inputs, while emission intensity of 2.4×10^5 was used as the threshold value for monitoring at 400 or 445 nm. Figure 11a reveals that, in the absence of chemical input $\mathbf{G_2}$ (input 1) and $\mathbf{G_3}$ (input 2), the emission intensities at 400 nm were very low. In the presence of either $\mathbf{G_2}$ or $\mathbf{G_3}$ or both, the emission response at 400 nm was higher due to the effective interruption of the PET process. Among different guest fragments, $\mathbf{G_3}$ having higher preference toward **H** than that of $\mathbf{G_2}$ would displace $\mathbf{G_2}$ from $\mathbf{H.G_2}$ to form $\mathbf{H.G_3}$ with an associated emission response that is typical for anthracene moiety, which could be attributed to the FRET process between $\text{pyrene}_{\mathbf{H}}$ donor and $\text{anthracene}_{\mathbf{G_3}}$ as acceptor. Emission responses at 445 nm in the presence of two inputs $\mathbf{G_2}$ (input 1) and $\mathbf{G_3}$ (input 2) were correlated for constructing a truth table that could describe a binary logic operation like $\text{TRANSFER}_{\mathbf{G_3}}$, and this could be extended for solution responses of **H** on silica surfaces (Figures 11a–d). In turn, the fluorescence output at 445 nm mimicked $\text{TRANSFER}_{\mathbf{G_3}}$ being only 1 when $\mathbf{G_3}$ is present, while emission responses at 400 nm could be used to describe a two input OR gate too (Figures 11). The change of luminescence intensity at 400 nm was monitored as output by using $\mathbf{G_2}$ (input 1) and $\mathbf{G_3}$ (input 2). The OR gate is generally switched on when either one or both inputs are present.

CONCLUSION

In summary, we have studied in detail the inclusion complex formation of an aza-macrocyclic host **H** with different two guest molecules ($\mathbf{G_1}$ and $\mathbf{G_2}$) having a pendent imidazolium ion. ^{1}H NMR studies have helped in establishing the relative spatial orientation/conformation of the individual host and guest moieties in the supramolecular assemblies ($\mathbf{H.G_1}$ and $\mathbf{H.G_2}$). These studies have also confirmed a favorable spatial orientation of pyrene of the host molecule and naphthalene (for $\mathbf{G_1}$) or coumarin (for $\mathbf{G_2}$) in $\mathbf{H.G_1}$ or $\mathbf{H.G_2}$ for FRET based energy transfer process to be operational. FRET based energy transfer is also confirmed from the results of the time-resolved emission studies. Thermodynamic feasibility for such energy transfer is ascertained from data obtained from steady

DOI: 10.1021/acs.joc.6b01631
J. Org. Chem. 2016, 81, 8977–8987

state redox potential and the evaluation of the E_{0-0} value for the respective molecule. Binding stoichiometry and association constant for each inclusion complex are evaluated by fluorescence and/or ITC studies. Differences in the affinity of the respective guest molecules ($\mathbf{G_1}$, $\mathbf{G_2}$, $\mathbf{G_3}$, and C18O6) and K^+ toward **H** as well as the differences in affinities for K^+ toward **H** and C18O6 have been utilized in demonstrating the self-sorting phenomenon with distinctly different luminescence responses. Such modulation in luminescence responses could be correlated in describing certain simple as well as complicated binary logic operations. Interestingly, such logic operations could be demonstrated based on the luminescence responses of the silica surfaces modified with **H** in the presence of various inputs. Thus, results described in the present study may provide a perspective for designing molecular devices for performing complicated logic functions. Such an example for supramolecular assembly on solid surface is scarce in the contemporary literature.

EXPERIMENTAL SECTION

Materials. 1-Methylimidazole, 2-bromonaphthalene, 4-bromomethyl-7-methoxycoumarin derivative, and C18O6 were purchased and used without any further purification. All solvents were purchased from commercial suppliers and used without any further purification. Column chromatography was performed on silica gel 100−200 mesh. **H** and $\mathbf{G_3}$ were synthesized as per previous reported procedures. Details about the various characterization data for **H** and $\mathbf{G_3}$ are presented in the Supporting Information.

Electrochemical Measurements. Cyclic voltammograms were recorded using a three electrode system. A platinum electrode was used as the working electrode. A platinum wire served as the counter electrode and a saturated $Ag/AgNO_3$ as a reference electrode. A ferrocene/ferrocenium redox couple was used as the internal standard. All solutions were thoroughly purged with nitrogen gas prior to the electrochemical measurements.

ITC Measurements. ITC experiments were performed at 25 °C in dichloromethane. In each run 2 μL was injected with a stirring speed 1000 rpm into the solution of host. A control experiment was done to determine the heat of dilution by carrying out the same experiment without host. Actual enthalpies were calculated by subtracting the control experiment enthalpy. All thermodynamic parameters were obtained by using a one site binding model. Errors of binding constant are in the range of ±10%. Errors in ΔG amount to 0.4 kcal, while errors in ΔH and $T\Delta S$ are higher due to uncertainties in the fitting procedure.

Spectral Measurements. The absorption and emission spectra were acquired at room temperature (25 °C). All spectral measurements have been carried out with freshly prepared solutions in quartz cuvette of 1.0 cm path length. Fluorescence lifetimes were measured by time correlated single photon counting (TCSPC), using a nanosecond diode LED source, 295 nm LED excitation source, and 310 and 340 nm LASER as the light source to trigger the fluorescence decay. The decays were analyzed on Data station-v6 decay analysis software. The acceptability of these fits was evaluated by χ^2 criteria and visual inspection of the residuals of the fitted function of the data. All NMR spectra were recorded with TMS as an internal standard on 500 MHz FT NMR at room temperature (25 °C). Fluorescence quantum yield (Φ_f) was determined using naphthalene and pyrene as a reference by employing the following equation:

$$\Phi_f = \Phi_{f'}(I_S/I_R)(A_R/A_S)(\eta^2{}_S/\eta^2{}_S)$$

in which I_i is the integrated area under the fluorescence curve, A_i denotes the absorption, η_i is the refractive index of the medium, and Φ_i is the fluorescence quantum yield. The subscripts i = S and R refer to the parameters corresponding to the sample and reference compound, respectively.

Synthetic Procedure of ***H.*** The methodology adopted for the synthesis of **H** was discussed earlier.[12a] Yield: 490 mg (60%). Sticky brown mass. ^{1}H NMR (500 MHz, $CDCl_3$, ppm): 2.73 (4H, t, J = 5.5 Hz), 3.43−3.49 (8H, m), 3.57−3.62 (4H, m), 3.71 (4H, t, J = 4.5 Hz), 3.95−4.00 (4H, m), 4.15 (2H, s), 6.76 (4H, d, J = 4.8 Hz), 7.76−7.87 (4H, m), 7.90−7.93 (2H, m), 7.95−8.01 (2H, m), 8.48 (1H, d, J = 9 Hz).[13] ^{13}C NMR (125 MHz, $CDCl_3$, ppm): 149.1, 131.3, 130.9, 130.7, 129.9, 128.3, 127.5, 127.1, 125.8, 125.0, 124.9, 124.8, 124.4, 121.6, 114.6, 71.1, 70.6, 69.9, 69.6, 69.3, 58.3, 54.2. HRMS (ESI−TOF) m/z: $[M + H]^+$ calculated for $C_{35}H_{40}NO_6$, 570.2811; found 570.2850.

Synthetic Procedure of $\mathbf{G_1}$. The methodology adopted for the synthesis of $\mathbf{G_1}$ was discussed earlier.[18b] White powder solid. Yield: 670 mg (80%). ^{1}H NMR (500 MHz, CD_3CN, ppm): 3.84 (3H, s), 5.50 (2H, s), 7.39 (1H, s), 7.45 (1H, s), 7.47 (1H, d, J = 5 Hz), 7.60−7.62 (2H, m), 7.93−8.00 (4H, m), 8.52 (1H, s). ^{13}C NMR (125 MHz, CD_3CN, ppm): 36.0, 53.0, 122.4, 124.0, 125.6, 127.0, 127.1, 127.8, 128.0, 128.2, 129.1, 131.2, 133.2, 133.3, 136.2. HRMS (ESI−TOF) m/z: $[M - PF_6^-]^+$ calculated for $C_{15}H_{15}N_2^+$, 223.1235; found 223.1230. Melting point: 85 °C.

Synthetic Procedure of $\mathbf{G_2}$. A solution of 1-methylimidazole (184 mg, 2.22 mmol) and 4-(bromomethyl)-7-methoxy-2*H*-chromen-2-one (600 mg, 2.22 mmol) in 50 mL of toluene was refluxed until a large amount of insoluble product occurred. The insoluble compound was isolated and washed with toluene. Then the insoluble residue was treated with aqueous solution of NH_4PF_6. White precipitate appeared after overnight stirring. Precipitate was washed with cold water. Yield: 760 mg (82%). ^{1}H NMR (500 MHz, CD_3CN, ppm): 3.88 (3H, s), 3.95 (3H, s), 5.55 (2H, s), 5.78 (1H, s), 6.89 (1H, s), 6.94 (1H, d, J = 10 Hz), 7.40(2H, d, J = 5 Hz), 7.50 (1H, d, J = 10 Hz), 8.66 (1H, s). ^{13}C NMR (125 MHz, CD_3CN, ppm): 36.3, 48.9, 55.9, 101.4, 110.9, 112.5, 117.4,123.1, 124.5, 125.1, 137.0, 148.2, 155.6, 160.1, 163.5. HRMS (ESI−TOF) m/z: $[M - PF_6^-]^+$ calculated for $C_{15}H_{15}N_2O_3^+$, 271.1083; found 271.1078. Melting point: 182 °C.

Synthetic Procedure of $\mathbf{G_3}$. The methodology adopted for the synthesis of $\mathbf{G_3}$ was discussed earlier.[12a] Yield: 450 mg (60%). Light yellow crystalline solid.[1] ^{1}H NMR (500 MHz, DMSO-d_6, ppm): 9.62 (2H, broad signal), 8.77 (1H, s), 8.25 (2H, d, J = 10.0 Hz), 8.17 (2H, d, J = 10.0 Hz), 7.70−7.69 (2H, m), 7.60 (4H, t, J = 8.0 Hz), 7.51−7.50 (3H, m), 5.12 (2H, s), 4.50 (2H, s). ^{13}C NMR (125 MHz, DMSO-d_6, ppm): 42.0, 51.3, 123.5, 124.6, 125.9, 127.4, 129.2, 129.5, 129.6, 130.2, 131.0, 131.3, 132.4. HRMS (ESI−TOF) m/z: $[M - PF_6^-]^+$ calculated for $C_{22}H_{20}N^+$, 298.1590; found 298.1573. Melting point:185 °C

ASSOCIATED CONTENT

Supporting Information

The Supporting Information is available free of charge on the ACS Publications website at DOI: 10.1021/acs.joc.6b01631.

Spectral characterization data, ^{13}C NMR, 2D NMR, and mass spectra, and absorption and emission spectral data (PDF)

AUTHOR INFORMATION

Corresponding Author

*E-mail: a.das@csmcri.org.

Notes

The authors declare no competing financial interest.

ACKNOWLEDGMENTS

M.G. and A.M. acknowledge Council of Scientific and Industrial Research (CSIR), India, for research fellowships. A.D. acknowledges a SERB (India) grant (SB/S1/IC-23/2013) and a CSIR-CSMCRI network project (CSC 0134) for funding.

DOI: 10.1021/acs.joc.6b01631
J. Org. Chem. 2016, 81, 8977−8987

REFERENCES

(1) (a) Whitesides, G. M.; Boncheva, M. *Proc. Natl. Acad. Sci. U. S. A.* **2002**, *99*, 4769−4774. (b) Biedermann, F.; Schneider, H.-J. *Chem. Rev.* **2016**, *116*, 5216−5300. (c) Peng, H.-Q.; Niu, L.-Y.; Chen, Y.-Z.; Wu, L.-Z.; Tung, C.-H.; Yang, Q.-Z. *Chem. Rev.* **2015**, *115*, 7502−7542. (d) Schalley, C. A.; Beizai, K.; Vögtle, F. *Acc. Chem. Res.* **2001**, *34*, 465−476. (e) Hernandez, J. V.; Kay, E. R.; Leigh, D. A. *Science* **2004**, *306*, 1532−1537. (f) Scarso, A.; Onagi, H.; Rebek, J., Jr. *J. Am. Chem. Soc.* **2004**, *126*, 12728−12729.

(2) (a) Ashton, P. R.; Chrystal, E. J. T.; Glink, P. T.; Menzer, S.; Schiavo, C.; Spencer, N.; Stoddart, J. F.; Tasker, P. A.; White, A. J. P.; Williams, D. J. *Chem. - Eur. J.* **1996**, *2*, 709−726. (b) Huang, F.; Gibson, H. W. *Prog. Polym. Sci.* **2005**, *30*, 982−1018. (c) Smith, A. C.; Macartney, D. H. *J. Org. Chem.* **1998**, *63*, 9243−9251. (d) Xue, M.; Yang, Y.; Chi, X.; Yan, X.; Huang, F. *Chem. Rev.* **2015**, *115*, 7398−7501.

(3) (a) Fahrenbach, A. C.; Zhu, Z. X.; Cao, D.; Liu, W. G.; Li, H.; Dey, S. K.; Basu, S.; Trabolsi, A.; Botros, Y. Y.; Goddard, W. A., III; Stoddart, J. F. *J. Am. Chem. Soc.* **2012**, *134*, 16275−16288. (b) Saha, S.; Flood, A. H.; Stoddart, J. F.; Impellizzeri, S.; Silvi, S.; Venturi, M.; Credi, A. *J. Am. Chem. Soc.* **2007**, *129*, 12159−12171. (c) Zhang, H.; Wang, Q.; Liu, M.; Ma, X.; Tian, H. *Org. Lett.* **2009**, *11*, 3234−3237.

(4) (a) Credi, A.; Balzani, V.; Langford, S. J.; Stoddart, J. F. *J. Am. Chem. Soc.* **1997**, *119*, 2679−2681. (b) Jiang, W.; Han, M.; Zhang, H. Y.; Zhang, Z. J.; Liu, Y. *Chem. - Eur. J.* **2009**, *15*, 9938−9945. (c) Semeraro, M.; Credi, A. *J. Phys. Chem. C* **2010**, *114*, 3209−3214. (d) Hansen, S. W.; Stein, P. C.; Sorensen, A.; Share, A. I.; Witlicki, H. W.; Kongsted, J.; Flood, A. H.; Jeppesen, J. O. *J. Am. Chem. Soc.* **2012**, *134*, 3857−3863. (e) Rogez, G.; Ferrer Ribera, B.; Credi, A.; Ballardini, R.; Gandolfi, M. T.; Balzani, V.; Liu, Y.; Northrop, B. H.; Stoddart, J. F. *J. Am. Chem. Soc.* **2007**, *129*, 4633−4642.

(5) (a) Webber, S. E. *Chem. Rev.* **1990**, *90*, 1469−1482. (b) Fox, M. A. *Acc. Chem. Res.* **1992**, *25*, 569−574. (c) Heilemann, M.; Tinnefeld, P.; Sanchez Mosteiro, G.; Garcia Parajo, M.; Van Hulst, N. F.; Sauer, M. *J. Am. Chem. Soc.* **2004**, *126*, 6514−6515.

(6) (a) Mandal, A. K.; Gangopadhyay, M.; Das, A. *Chem. Soc. Rev.* **2015**, *44*, 663−676. (b) Xia, B.; Zheng, B.; Han, C.; Dong, S.; Zhang, M.; Hu, B.; Yu, Y.; Huang, F. *Polym. Chem.* **2013**, *4*, 2019−2024. (c) Dong, S.; Zheng, B.; Yao, Y.; Han, C.; Yuan, J.; Antonietti, M.; Huang, F. *Adv. Mater.* **2013**, *25*, 6864−6867.

(7) Lehn, J. M.; Vierling, P.; Hayward, R. C. *J. Chem. Soc., Chem. Commun.* **1979**, 296−298.

(8) Castillo, D.; Astudillo, P.; Mares, J.; Gonzalez, F. J.; Vela, A.; Tiburcio, J. *Org. Biomol. Chem.* **2007**, *5*, 2252−2256.

(9) Lee, M.; Niu, Z.; Schoonover, D. V.; Slebodnick, C.; Gibson, H. W. *Tetrahedron* **2010**, *66*, 7077−7082.

(10) (a) Noujeim, N.; Leclercq, L.; Schmitzer, A. R. *J. Org. Chem.* **2008**, *73*, 3784−3790. (b) Yao, Y.; Chi, X.; Zhou, Y.; Huang, F. *Chem. Sci.* **2014**, *5*, 2778−2782. (c) Zhang, Z.; Zhao, Q.; Yuan, J.; Antonietti, M.; Huang, F. *Chem. Commun.* **2014**, *50*, 2595−2597. (d) Zhou, Y. J.; Yao, Y.; Xue, M. *Chem. Commun.* **2014**, *50*, 8040−8042.

(11) (a) Suresh, M.; Mandal, A. K.; Kesharwani, M. K.; Adarsh, N. N.; Ganguly, B.; Kanaparthi, R. K.; Samanta, A.; Das, A. *J. Org. Chem.* **2011**, *76*, 138−144. (b) Suresh, M.; Mandal, A. K.; Suresh, E.; Das, A. *Chem. Sci.* **2013**, *4*, 2380−2386.

(12) (a) Mandal, A. K.; Suresh, M.; Kesharwani, M. K.; Gangopadhyay, M.; Agrawal, M.; Boricha, V. P.; Ganguly, B.; Das, A. *J. Org. Chem.* **2013**, *78*, 9004−9012. (b) Mandal, A. K.; Das, P.; Mahato, P.; Acharya, S.; Das, A. *J. Org. Chem.* **2012**, *77*, 6789−6800.

(13) (a) Kompa, K. L.; Levine, R. D. *Proc. Natl. Acad. Sci. U. S. A.* **2001**, *98*, 410−414. (b) de Silva, A. P.; McClenaghan, N. D. *Chem. - Eur. J.* **2004**, *10*, 574−586. (c) Szacilowski, K.; Macyk, W.; Stochel, G. *J. Am. Chem. Soc.* **2006**, *128*, 4550−4551.

(14) (a) Barrett, E. S.; Dale, T. J.; Rebek, J., Jr. *J. Am. Chem. Soc.* **2008**, *130*, 2344−2350. (b) Rudzevich, Y.; Rudzevich, V.; Klautzsch, F.; Schalley, C. A.; Böhmer, V. *Angew. Chem., Int. Ed.* **2009**, *48*, 3867−3871.

(15) (a) Yamauchi, Y.; Yoshizawa, M.; Akita, M.; Fujita, M. *J. Am. Chem. Soc.* **2010**, *132*, 960−966. (b) Schmittel, M.; Mahata, K. *Chem. Commun.* **2010**, *46*, 4163−4165.

(16) (a) Shaller, A. D.; Wang, W.; Gan, H.; Li, A. D. Q. *Angew. Chem., Int. Ed.* **2008**, *47*, 7705−7709. (b) Ghosh, S.; Wu, A.; Fettinger, J. C.; Zavalij, P. Y.; Isaacs, L. *J. Org. Chem.* **2008**, *73*, 5915−5925. (c) Ghosh, S.; Li, X.-Q.; Stepanenko, V.; Würthner, F. *Chem. - Eur. J.* **2008**, *14*, 11343−11357. (d) Safont-Sempere, M. M.; Osswald, P.; Stolte, M.; Grüne, M.; Renz, M.; Kaupp, M.; Radacki, K.; Braunschweig, H.; Würthner, F. *J. Am. Chem. Soc.* **2011**, *133*, 9580−9591.

(17) (a) Chen, X.; Pradhan, T.; Wang, F.; Kim, J. S.; Yoon, J. *Chem. Rev.* **2012**, *112*, 1910−1956. (b) Bull, S. D.; Davidson, M. G.; van den Elsen, J. M. H.; Fossey, J. S.; Jenkins, A. T. A.; Jiang, Y.; Kubo, Y.; Marken, F.; Sakurai, K.; Zhao, J.; James, T. D. *Acc. Chem. Res.* **2013**, *46*, 312−326. (c) de Silva, A. P.; Gunaratne, H. Q. N.; Gunnlaugsson, T.; Huxley, A. J. M.; McCoy, C. P.; Rademacher, J. T.; Rice, T. E. *Chem. Rev.* **1997**, *97*, 1515−1566.

(18) (a) Kiviniemi, S.; Sillanpaa, A.; Nissinen, M.; Rissanen, K.; Lamsa, M. T.; Pursiainen, J. *Chem. Commun.* **1999**, 897−898. (b) Mandal, A. K.; Suresh, M.; Das, A. *Org. Biomol. Chem.* **2011**, *9*, 4811−4817.

(19) (a) Stolwijk, T. B.; Sudhoelter, E. J. R.; Reinhoudt, D. N.; Van Eerden, J.; Harkema, S. *J. Org. Chem.* **1989**, *54*, 1001−1005. (b) Li, L.; Clarkson, G. J. *Org. Lett.* **2007**, *9*, 497−500.

(20) (a) Chen, L.; Zhang, Y. M.; Liu, Y. *J. Phys. Chem. B* **2012**, *116*, 9500−9506. (b) Chen, L.; Zhang, H. Y.; Liu, Y. *J. Org. Chem.* **2012**, *77*, 9766−9773. (c) Douteau-Guével, N.; Coleman, A. W.; Morel, J.-P.; Morel-Desrosiers, N. *J. Chem. Soc., Perkin Trans. 2* **1999**, 629−633.

(21) (a) Whitesides, G. M.; Mathias, J. P.; Seto, C. T. *Science* **1991**, *254*, 1312−1319. (b) Wu, A.; Isaacs, L. *J. Am. Chem. Soc.* **2003**, *125*, 4831−4835. (c) Mukhopadhyay, P.; Wu, A.; Isaacs, L. *J. Org. Chem.* **2004**, *69*, 6157−6164. (d) He, Z.; Jiang, W.; Schalley, C. A. *Chem. Soc. Rev.* **2015**, *44*, 779−789. (e) Jiang, W.; Schalley, C. A. *Proc. Natl. Acad. Sci. U. S. A.* **2009**, *106*, 10425−10429. (f) Wang, F.; Han, C.; He, C.; Zhou, Q.; Zhang, J.; Wang, C.; Li, N.; Huang, F. *J. Am. Chem. Soc.* **2008**, *130*, 11254−11255.

(22) (a) Safont-Sempere, M. M.; Fernández, G.; Würthner, F. *Chem. Rev.* **2011**, *111*, 5784−5814. (b) Saha, M. L.; Schmittel, M. *Org. Biomol. Chem.* **2012**, *10*, 4651−4684. (c) Mukhopadhyay, P.; Zavalij, P. Y.; Isaacs, L. *J. Am. Chem. Soc.* **2006**, *128*, 14093−14102.

(23) (a) Frensdorff, H. K. *J. Am. Chem. Soc.* **1971**, *93*, 600−606. (b) Jiang, W.; Schalley, C. A. *Beilstein J. Org. Chem.* **2010**, *6*, 14.

DOI: 10.1021/acs.joc.6b01631
J. Org. Chem. 2016, 81, 8977−8987